Hindawi Publishing Corporation
Advances in Materials Science and Engineering
Volume 2013, Article ID 763838, 11 pages
http://dx.doi.org/10.1155/2013/763838

Research Article

Characterisation and Properties of Lithium Disilicate Glass Ceramics in the SiO_2-Li_2O-K_2O-Al_2O_3 System for Dental Applications

Naruporn Monmaturapoj, Pornchanok Lawita, and Witoon Thepsuwan

National Metal and Materials Technology Center, 114 Thailand Science Park, Pathumthani 12120, Thailand

Correspondence should be addressed to Naruporn Monmaturapoj; narupork@mtec.or.th

Received 29 April 2013; Revised 25 June 2013; Accepted 28 June 2013

Academic Editor: Delia Brauer

This work proposes four different glass formulas derived from the SiO_2-Li_2O-K_2O-Al_2O_3 system to investigate the effect of glass composition on their crystal formations and properties. Glass LD1 was SiO_2-Li_2O-K_2O-Al_2O_3 system with the addition of P_2O_5 and CaF_2 as nucleating agents. In Glass LD2, a slight amount of MgO was mixed in order to increase the viscosity of the melting glass. Finally, the important factor of Si : Li ratio was increased in Glasses LD3 and LD4 with compositions otherwise the same as LD1 and LD2. The results found that P_2O_5 and CaF_2 served as a nucleating site for lithium phosphate and fluorapatite to encourage heterogenous nucleation and produce a fine-grained interlocking microstructure of lithium disilicate glass ceramics. MgO content in this system seemed to increase the viscosity of the melting glass and thermal expansion coefficient including the chemical solubility. Increasing the Si : Li ratio in glass compositions resulted in the change of the microstructure of $Li_2Si_2O_5$ crystals.

1. Introduction

All-ceramic systems for dental restoration have been extensively used over recent years due to substantial developments meeting dental requirements, particularly in terms of their mechanical properties and the opaque, presently accessible appearance of all-ceramic materials [1]. Lithium disilicate glass ceramic ($Li_2Si_2O_5$) is one such all-ceramic system, currently used in the fabrication of single and multiunit dental restorations mainly for dental crowns, bridges, and veneers because of its color being similar to natural teeth and its excellent mechanical properties [2].

In general, glass ceramics can be produced by melting glass and converting the substance into a uniform nucleation and growth of fine-grained ceramics by controlled crystallization process, in which the crystalline phases are nucleated and grown in glass via heat treatment [3–5]. Lithium disilicate glass ceramic, in particular the Li_2O-SiO_2 system, is the first material classified as glass ceramic discovered by Stookey as having better mechanical properties over base glass [6]. Since then, many comprehensive studies have paid attention to the binary Li_2O-SiO_2 system [7–13]. However, this binary system lacks chemical durability for use as a restorative material in dentistry. Therefore, nonstoichiometric compositions or multicomponent glass ceramics were carried out to improve the chemical durability, especially the addition of Al_2O_3 and K_2O to the stoichiometric composition reported to enhance the chemical durability of this glass ceramic [14–16]. Several constituents, for example, ZnO, ZrO_2, CaO, and P_2O_5, were introduced to improve the properties of the final material [4, 17–20]. Also, it is noted that P_2O_5 as a nucleating agent plays an important role in phase formation and crystallization for lithium disilicate glass ceramic [16, 21, 22]. For that reason, a slight P_2O_5 content in glass composition could produce a fine-grained interlocking microstructure resulting in high mechanical strength [21].

Fluorine in glass affect its crystallization mechanism and the phases formation due to the fact that fluorine is a network modifier which could rearrange the glass network by forming nonbridging fluorine to replace nonbridging oxygens [6]. Fluorine in calcium phosphate glasses produces a fluorapatite phase which has less solubility characteristics; therefore, it

could improve the chemical solubility of the glass ceramic [23]. In addition, Beall [24] and Echeverria and Beall [18] suggested that the $SiO_2 : Li_2O$ ratio is also a key success factor in the formation of the main crystal phase in a new lithium disilicate glass ceramic system. In order to optimize the viscous properties of lithium disilicate glass to have better pressing ability, components such as La_2O_3 and MgO were added to the main composition [25, 26].

In fact, studies of lithium disilicate glass ceramics have focused mainly on the phase formation and crystallization of $Li_2Si_2O_5$, as affected by variations of temperature during the heat treatment cycle and of minor compositional changes in the main glass composition. These factors influence the microstructure of the glass ceramic and consequently affect the properties of the final products.

In this study, four different glass formulas derived from the SiO_2-Li_2O-K_2O-Al_2O_3 system were prepared to investigate the effect of glass compositions on their crystal formations, microstructures, and properties through the conventional glass melting process. P_2O_5 and CaF_2 as nucleating agents were introduced to induce heterogeneous nucleation and then produce a fine-grained interlocking microstructure after heat treatment. MgO was added in the glass system to increase the viscous properties, and, finally, the $SiO_2 : Li_2O$ ratio in the glass composition was increased. The experimental results and their discussion are addressed as concerns the crystallization behavior of the glasses, the microstructures, and properties of the glass ceramics with the potential to be used as dental restorations.

2. Materials and Methods

2.1. Glass Preparation. Glass batches were prepared by mixing appropriate amounts of SiO_2, Li_2CO_3, $MgCO_3$ (Sigma-Aldrich Company, Belgium), Al_2O_3 (Fluka Analytical, Germany), P_2O_5 (Acros organics, USA), K_2CO_3 (Fluka chemika, France), and CaF_2 (Merck chemicals, Germany). All starting materials were reagent grade. Glass batches according to glass compositions as shown in Table 1 were melted in a covered Pt-10%Rh crucible at 1500°C for 2 hrs and then quenched in cold water to make frit. To achieve homogeneity, glass frit was milled before being remelted at the same temperature for 2 hrs. The melting glass was cast into warm graphite molds to obtain glass rods with a dimension of 14 mm in diameter × 100 mm long. Graphite molds were annealed in a muffle furnace at 400–500°C for 2 hrs to reduce the internal stress in the glasses followed by cooling to room temperature at 1°C/min.

2.2. Heat Treatment. Samples were cut into several disks of 14 mm × 5 mm long and then heat-treated in a Lenton furnace (Lenton Ltd., Hope Valley, UK). A two-stage heat-treatment schedule was performed in which the glasses were heated to a nucleating temperature of 500°C with a heating rate of 5°C/min, held for 2 hrs, and then ramped up to various crystal growth temperatures (e.g., 700°C). The heating rate was 5°C/min, and samples were held for 2 hrs followed by furnace cooling with 5°C/min to room temperature. Following heat treatment, samples were referred to as glass ceramics LD1–LD4.

Table 1: Glass compositions (% mol).

Oxides	LD1	LD2	LD3	LD4
SiO_2	60.0	59.0	63.0	62.0
Li_2O	32.0	31.0	29.0	28.0
K_2O	1.0	1.0	1.0	1.0
Al_2O_3	2.0	2.0	2.0	2.0
P_2O_5	2.0	2.0	2.0	2.0
CaF_2	3.0	3.0	3.0	3.0
MgO	—	2.0	—	2.0
Total	100.0	100.0	100.0	100.0
$SiO_2 : Li_2O$	1.88	1.90	2.17	2.21

2.3. Thermal Analysis

2.3.1. Differential Thermal Analysis. A Netzsch thermal analysis (NETZSCH STA 449 F3, Germany) was used to determine T_g and T_c by heating to 1000°C with a heating rate of 10°C/min. Fine glass samples (6–10 μm) were analyzed under flowing nitrogen with a Pt crucible filled with alumina as reference and then heated together at the set up heating rate. The results were used as a guide for determining the heat treatment temperatures applied to induce crystallization.

2.3.2. Thermal Expansion Measurement. The coefficient of thermal expansion using a Netzsch thermal analysis (NETZSCH DIL 402 PC, Germany) dilatometer with a heating rate of 5°C/min was applied on the glass ceramic bars (5 mm × 5 mm × 25 mm) measuring from room temperature up to 600°C. The linear thermal expansion coefficient (α) was calculated using the general equation: $\alpha = (\Delta L/L) \cdot (1/\Delta T)$, where ($\Delta L$) is the increase in length, (ΔT) is the temperature interval over which the sample is heated, and (L) is the original length of the specimen.

2.4. X-Ray Diffraction Analysis. Phase analyses of the glasses and glass ceramics were performed by X-ray diffraction (XRD, Rigaku TTRAX III) operating from 10° to 70° 2θ at a scan speed of 2° 2θ/min and a step size of 0.02° 2θ with CuK_α radiation (K_α = 1.5406 nm) at 300 mA and 50 kV. Identification of phases was achieved by comparing the result diffraction patterns with the ICDD (JCPDS) standard.

2.5. Scanning Electron Microscopy. Microstructure of the glass ceramics was investigated by scanning electron microscope (SEM: Hitachi S-3400N). After heat treatment, the samples were polished with SiC paper (nos. 400, 800, 1000, 1200, and 2500) and finally with diamond paste (sizes 6, 3, and 1 μm). Then, the samples were edged by chemical etching process with hydrofluoric acid (4% vol) for 1 minute and cleaned afterwards with a high-frequency vibration. The samples were coated with gold by ion sputtering device (JEOL JFC-1200) at a current generation of 15 mA for 200 seconds.

2.6. Mechanical Properties Testing

2.6.1. Indentation Fracture Toughness (IFT). Glass specimens (Ø14 mm × 5 mm) were initially cut from the glass rod with

a diamond saw blade machine (IsoMet 4000, Buehler, Ltd., USA) to create parallel faces. After heat treatment, they were polished down using SiC paper and finally with diamond paste. Indentations were obtained using Vickers hardness testing machine (Vickers-Armstrong, Ltd., Crayford, UK) for loads of 1 kg, 2 kg, 3 kg, 5 kg, and 7.5 kg. The used loads were restricted to a range over which the indentation patterns remained well defined, at the lower end by the minimum requirement $c \geq 2a$, where c is the radial crack length and a is the indentation half-diagonal length, and at the upper end by chipping or by the limitation of specimen thickness. For each load, at least 15–20 indentations were made, and at least ten to fifteen readings were taken using an optical microscopy (ZEISS Model Axiotech) equipped with a digital camera and computer. Fracture toughness was calculated using the formula $K_{Ic} = 0.0824\ P/C^{3/2}$, where K_{Ic} is indentation fracture toughness (IFT), P is the indentation load, and C is the radial crack size.

2.6.2. Biaxial Flexural Strength. Glass specimens (Ø14 mm × 4 mm) were cut from the glass rods to obtain at least six disks. After two-stage heat treatment, they were ground and polished using SiC paper and diamond paste. Test geometry of three-ball supported test-jig equipped with a universal testing machine (Model 8872, Instron Instruments, Ltd., Fareham, Hampshire, UK) with a ring support of 10 mm at a cross-head speed of 1 mm/min was performed on the samples (Figure 1). A sheet of paper was placed between the samples and support ring to eliminate any additional flatness and reduce friction [27]. The center of each disk was marked as the correct place for the loading ball before testing. The maximum stress, σ_{max} at the center was calculated applying the following equation [27]:

$$\sigma_{max} = \frac{3(1+\nu)P}{4\pi t^2}\left[1 + 2\ln\frac{a}{b} + \frac{(1-\nu)}{(1+\nu)}\left\{1 - \frac{b^2}{2a^2}\right\}\frac{a^2}{R^2}\right], \quad (1)$$

where P is load, t is disk thickness, a is the radius of the circle of the support ring, b is the radius of the region of uniform loading at the center $b = t/3$, R is the radius of the disk sample, and ν is Poisson's ratio, $\nu = 0.25$.

2.7. Chemical Solubility Testing. After two-stage heat treatment, the glass specimens (Ø14 mm × 2 mm) were polished to create parallel faces. Glass ceramic specimens were washed and dried at 150°C for 4 hrs followed by being weighed to the nearest 0.1 mg (W_b). The total surface area of the specimens was determined to the nearest 0.1 cm^2. Specimens were then individually immersed in a 250 mL glass bottle with 100 mL acetic acid, 4% solution in water. The bottles were closed with their caps and then placed in an oven at 80°C for 16 hrs. Next, the specimens were washed and dried at 150°C for 4 hrs to achieve a constant mass. Finally, the specimens were reweighed to obtain the mass after immersion (W_a). The chemical solubility was determined by the following equation:

$$\text{Chemical solubility} = \frac{(W_b - W_a)}{\text{surface area of the specimen}}. \quad (2)$$

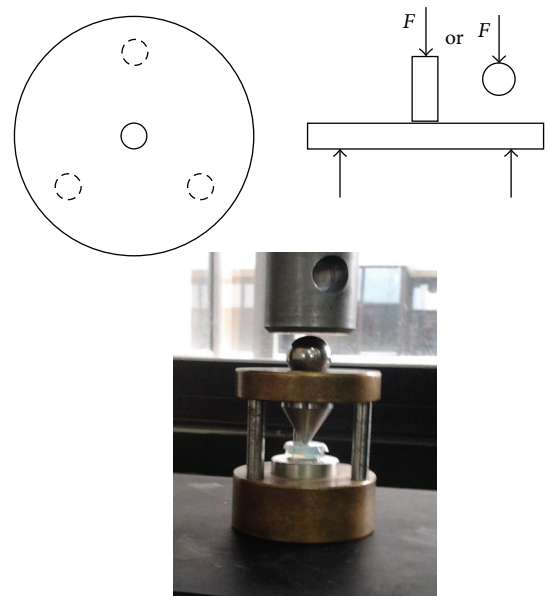

Figure 1: Test geometry of biaxial flexural strength.

Table 2: Summary of transition and crystallization temperatures of glasses.

Glasses	T_g (°C)	1st T_c (°C)	2nd T_c (°C)	3rd T_c (°C)
LD1	520	650	870	910
LD2	530	645	860	910
LD3	505	650	910	—
LD4	500	650	770	885

The chemical solubility test method in this study was referred to the ISO 6872 [28].

3. Results and Discussion

3.1. Differential Thermal Analysis. The DTA traces for glasses LD1–LD4 in Figure 2 and the summary of the exothermic and endothermic peaks in Table 2 show the exothermic and endothermic anomalies for all glasses attributed to either the glass transition (T_g) or crystallization temperatures (T_c).

The DTA traces of Glass LD1 exhibited triple exothermic peaks at 650°C, 860°C, and 910°C. A similar trend of three crystallization peaks at 650°C, 860°C, and 910°C was observed in Glass LD2. The study by Schweiger et al. [29] reported that the first crystallization of SiO_2-Li_2O system founds at 589°C corresponding to Li_2SiO_3 and the second crystallization peak at 770°C associated to $Li_2Si_2O_5$. The first and second crystallization temperatures of Li_2O-Al_2O_3-SiO_2 system in this study were at a higher temperature than the stoichiometric composition. This might be because of the addition of P_2O_5 and CaF_2 into glass compositions. Then, the third exothermic peak was observed. The addition of the MgO may not result in any significant changes in the T_g and T_c of the Glasses LD1 and LD2.

In Glass LD3, T_cs were observed at 650°C and 910°C. Two exothermic peaks associated with the crystallization

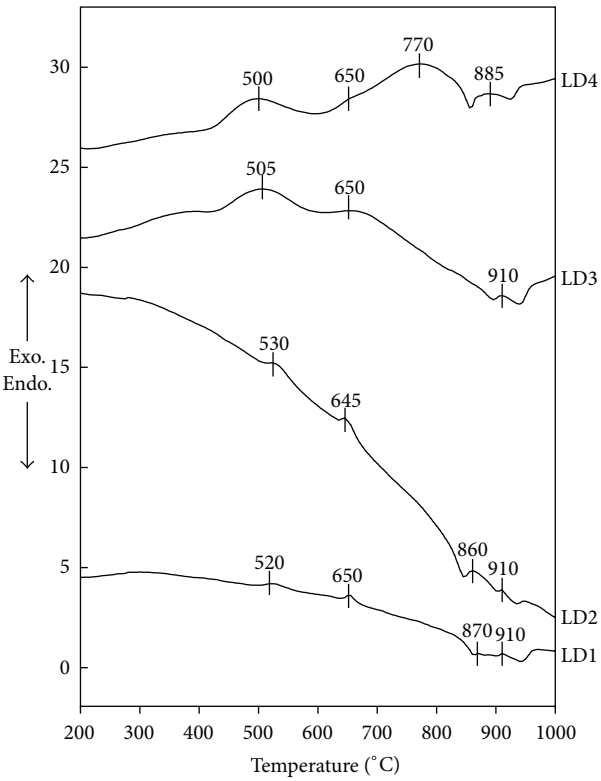

Figure 2: DTA traces of Glasses LD1–LD4.

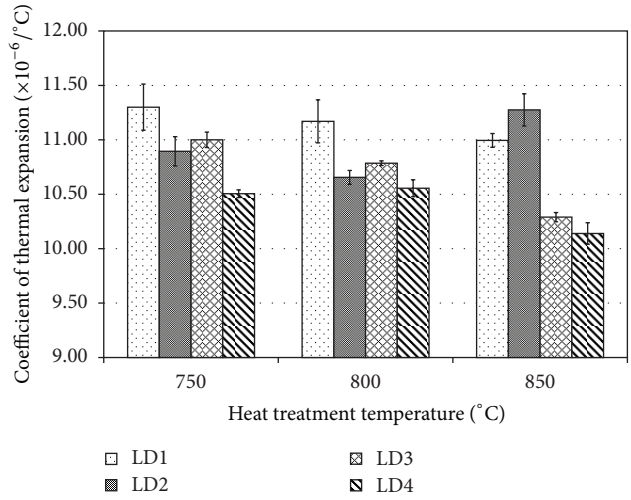

Figure 3: The coefficient of thermal expansion of LD1, LD2, LD3, and LD4 which were heat-treated at 750–850°C for 2 hrs.

temperatures were observed by increasing the Si : Li ratio in LD3. Differently, in Glass LD4, three exothermic peaks were observed: firstly, a small peak at about 650°C and two broadening peaks at 770°C and 885°C. It seems that the second crystallization temperature decreased to 770°C in this composition. The addition of MgO in LD4 was behind the decrease of the second crystallization down to a lower temperature than that of LD1 and LD2 which had lower $SiO_2 : Li_2O$ ratios. Moreover, the crystallization of fluorapatite, Li_3PO_4, and aluminosilicate is the minor crystallization in the system, so that it is difficult to identify the exothermic peaks related to these minor phases.

3.2. The Coefficient of Thermal Expansion. Figure 3 presents the changes in thermal expansion coefficients of glass ceramics as a function of heat treatment temperatures. The coefficients of thermal expansion for LD1–LD4 decreased with increasing heat treatment temperature in all glass ceramic samples except LD2, of which the thermal expansion coefficient rose following heat treatment at 850°C.

The increasing in thermal expansion coefficient value of LD2 after heat treatment at 850°C was possibly due to the addition of MgO. It is well known that MgO is not a glass former; therefore, the addition of MgO causes a weakening of the glass network structure and, consequently, a higher coefficient of thermal expansion [30]. Even though MgO was also added in LD4, the thermal expansion coefficient of LD4 after heat treatment at 850°C was decreased. The possible reason to explain this phenomenon is the different in $SiO_2 : Li_2O$ ratio. The $SiO_2 : Li_2O$ ratio of LD4 was 2.21, which was higher than that of LD2 (1.90).

In general, the thermal expansion coefficients of the glass ceramics mainly depend on the crystalline phases present at different temperatures and volume content in the matrix glass. Not only crystal types affect the thermal expansion coefficient but also the glass composition which is related to the structure of the glass [31]. The different crystal types have different thermal expansion coefficients [32]. The explanation behind the high thermal expansion coefficient of all glass ceramics in this study is the presence of several crystalline phases such as fluorapatite (10.0×10^{-6}/°C [33]), lithium phosphate, lithium metasilicate (13.0×10^{-6}/°C [34]) and lithium disilicate (11.4×10^{-6}/°C [34]), which have a high thermal expansion coefficient in the glass composition. The decrease of the thermal expansion coefficient as the temperature rise can be explained by the β-quartz solid solution changes into lithium aluminium silicate: virgilite (a stuffed β-quartz), having a low or negative thermal expansion coefficient with the temperature increasing [35].

3.3. Summary of the Phase Evolution. Figure 4 shows XRD patterns of all glass ceramics heat treated at 700–850°C for 2 hrs, and the crystalline phases are summarized in Table 3. The crystal structures found in LD1 heat treated at 700°C were lithium disilicate (LD, $Li_2Si_2O_5$: ICDD no. 40-0376), lithium metasilicate (LS, Li_2SiO_3: ICDD no. 29-0829), lithium aluminium silicate (virgilite, $Li_{0.6}Al_{0.6}Si_{2.4}O_6$: ICDD no. 21-0503 and spodumene ($LiAlSi_2O_6$: ICDD no. 033-0786), fluorapatite ($Ca_5(PO_4)_3F$: ICDD no. 15-0876), lithium phosphate (Li_3PO_4: 015-0760), and SiO_2: high quartz (2θ = 20.26°, ICDD no. 11-0252). At higher temperatures, the intensity of LS and virgilite peaks decreased while the intensity of lithium disilicate peaks increased. This exhibited higher in lithium disilicate crystallization. In addition, the peaks of β-quartz decreased until disappeared when heat treated at 850°C.

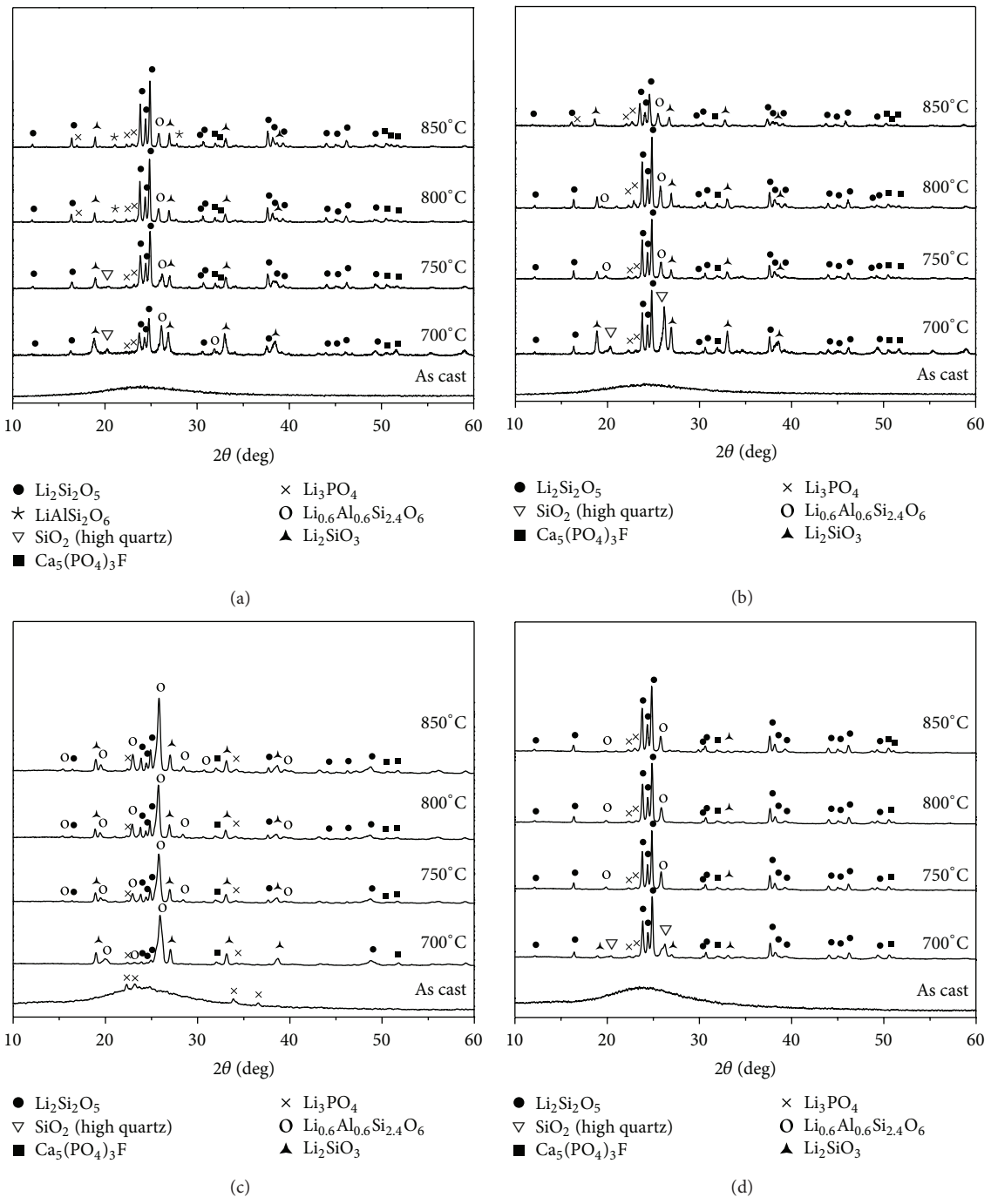

Figure 4: X-ray diffraction patterns of (a) LD1, (b) LD2, (c) LD3, and (d) LD4 after heat treatment at 700–850°C for 2 hrs.

A similar phase formation was also observed in LD2 with the addition of MgO. The small discrepancy was the crystal peaks associated to β-quartz solid solution (2θ = 26.26°) when heat treatment at 700°C transformed into virgilite (2θ = 25.88°) after heat treatment at 750°C. And this phase remained when heat treatment was at 800°C and 850°C.

Generally, the β-quartz could be stabilized by Li^+ or Mg^{2+}, Zn^+, and Al^{3+} called quartz-solid-solution which normally does not transform into the low-quartz-solid-solution while cooling down to room temperature resulting of a small thermal expansion coefficient [36]. Meanwhile, virgilite is the naturally occurring representative of the solid-solution series between β-quartz and $LiAlSi_2O_6$ with a stuffed β-quartz structure [34]. However, the possible explanation of the virgilite formation in laboratory experiment was that the sluggish reaction rates in the system Li_2O-Al_2O_3-SiO_2 require high pressure and temperature. Then reaction rate could be increased by the presence of Fe, alkalis, and volatiles, thus promoting the formation of virgilite at lower pressure within its stability field [34].

Table 3: Summary of crystalline phases.

Glasses	Heat treatment temperature (°C)	Crystalline phases
LD1	700	$Li_2Si_2O_5$, Li_2SiO_3, $Li_{0.6}Al_{0.6}Si_{2.4}O_6$, Li_3PO_4, $Ca_5(PO_4)_3F$, SiO_2
	750	$Li_2Si_2O_5$, Li_2SiO_3, $Li_{0.6}Al_{0.6}Si_{2.4}O_6$, Li_3PO_4, $Ca_5(PO_4)_3F$, SiO_2
	800	$Li_2Si_2O_5$, Li_2SiO_3, $Li_{0.6}Al_{0.6}Si_{2.4}O_6$, Li_3PO_4, $Ca_5(PO_4)_3F$
	850	$Li_2Si_2O_5$, Li_2SiO_3, $Li_{0.6}Al_{0.6}Si_{2.4}O_6$, $LiAlSi_2O_5$, Li_3PO_4, $Ca_5(PO_4)_3F$
LD2	700	$Li_2Si_2O_5$, Li_2SiO_3, $Li_{0.6}Al_{0.6}Si_{2.4}O_6$, Li_3PO_4, $Ca_5(PO_4)_3F$, SiO_2
	750	$Li_2Si_2O_5$, Li_2SiO_3, $Li_{0.6}Al_{0.6}Si_{2.4}O_6$, Li_3PO_4, $Ca_5(PO_4)_3F$
	800	$Li_2Si_2O_5$, Li_2SiO_3, $Li_{0.6}Al_{0.6}Si_{2.4}O_6$, Li_3PO_4, $Ca_5(PO_4)_3F$
	850	$Li_2Si_2O_5$, Li_2SiO_3, $Li_{0.6}Al_{0.6}Si_{2.4}O_6$, Li_3PO_4, $Ca_5(PO_4)_3F$
LD3	700	$Li_2Si_2O_5$, Li_2SiO_3, $Li_{0.6}Al_{0.6}Si_{2.4}O_6$, Li_3PO_4, $Ca_5(PO_4)_3F$, SiO_2
	750	$Li_2Si_2O_5$, Li_2SiO_3, $Li_{0.6}Al_{0.6}Si_{2.4}O_6$, Li_3PO_4, $Ca_5(PO_4)_3F$
	800	$Li_2Si_2O_5$, Li_2SiO_3, $Li_{0.6}Al_{0.6}Si_{2.4}O_6$, Li_3PO_4, $Ca_5(PO_4)_3F$
	850	$Li_2Si_2O_5$, Li_2SiO_3, $Li_{0.6}Al_{0.6}Si_{2.4}O_6$, Li_3PO_4, $Ca_5(PO_4)_3F$
LD4	700	$Li_2Si_2O_5$, Li_2SiO_3, $Li_{0.6}Al_{0.6}Si_{2.4}O_6$, Li_3PO_4, $Ca_5(PO_4)_3F$, SiO_2
	750	$Li_2Si_2O_5$, Li_2SiO_3, $Li_{0.6}Al_{0.6}Si_{2.4}O_6$, Li_3PO_4, $Ca_5(PO_4)_3F$
	800	$Li_2Si_2O_5$, Li_2SiO_3, $Li_{0.6}Al_{0.6}Si_{2.4}O_6$, Li_3PO_4, $Ca_5(PO_4)_3F$
	850	$Li_2Si_2O_5$, Li_2SiO_3, $Li_{0.6}Al_{0.6}Si_{2.4}O_6$, Li_3PO_4, $Ca_5(PO_4)_3F$

Figure 4(c) presents XRD pattern of LD3 heat treatment at different temperatures. By increasing the $SiO_2 : Li_2O$ ratio, in the glass composition, phase separation occurred due to the white and semiopaque appearance observed in LD3. Therefore, the crystal structures found in the as-cast glass were Li_3PO_4. At 700°C, XRD patterns showed the phase formation of Li_2SiO_3, lithium aluminium silicate, $Li_2Si_2O_5$, $Ca_5(PO_4)_3F$, and SiO_2: high quartz. The small peaks of Li_3PO_4 decreased when heat treated at higher temperatures. With increasing temperature, the intensity of $Li_2Si_2O_5$ increased as well as the retention of Li_2SiO_3, lithium aluminium silicate (virgilite), and $Ca_5(PO_4)_3F$. By increasing the $SiO_2 : Li_2O$ ratio, the more lithium aluminium silicate crystal peaks were observed compared to LD1 which has low $SiO_2 : Li_2O$ ratio.

The phase formation of LD4 is presented in Figure 4(d). The as-cast glass appearance looks clearer than that of LD3, implying that no phase separation occurred in this glass. At 700°C, the peaks corresponded to Li_2SiO_3, Li_3PO_4, $Li_2Si_2O_5$, $Ca_5(PO_4)_3F$, lithium aluminium silicate, and SiO_2 in the form of the high quartz observed. Then after heat treatment at higher temperature, the crystal peaks associated to β-quartz solid solution ($2\theta = 26.26^\circ$) when heat-treated at 700°C transformed into virgilite ($2\theta = 25.88^\circ$) after heat treatment at 750°C; this is similar to LD2. The difference from LD2 was the number of Li_2SiO_3 peaks observed in LD4 wich was less than that in LD2.

The growth of lithium disilicate could be initiated by the primary crystallization of the precursor lithium metasilicate, in particular, lithium disilicate glass ceramic containing Al_2O_3 [36]. Glass ceramic containing P_2O_5 may be nucleated by the initiation of the phase separation process, such as Li_3PO_4 nuclei [4, 37, 38]. P_2O_5 can react with Li_2O in Li_2O-rich regions to form the Li_3PO_4 crystal nuclei which act as nucleating sites shown in reaction(3). Some Li_2O was consumed in the Li_2O-rich regions to form Li_3PO_4 phase (reaction (3)) which can induce the precipitation of Li_2SiO_3 crystal (reaction(4)). It is reasonable to assume that Li_2SiO_3 precipitated on the Li_3PO_4 crystal nuclei in Li-rich regions, and the growth of $Li_2Si_2O_5$ was at the expense of consuming Li_2SiO_3 as shown in reaction (5)

$$P_2O_5\ (\text{glass}) + 3Li_2O\ (\text{glass}) = 2\ Li_3PO_4\ (\text{crystal}) \quad (3)$$

$$Li_2O\ (\text{glass}) + SiO_2\ (\text{glass}) = Li_2SiO_3\ (\text{crystal}) \quad (4)$$

$$Li_2SiO_3\ (\text{crystal}) + SiO_2\ (\text{glass}) = Li_2Si_2O_5\ (\text{crystal}). \quad (5)$$

Therefore, the sequence of the primary crystal phase formation as Li_3PO_4, Li_2SiO_3, and $Li_2Si_2O_5$ was proposed [4]. On the other hand, the investigation on complex simultaneous and sequential solid-state reactions in an Al_2O_3-free lithium disilicate glass ceramic found that Li_3PO_4 crystals were formed after the crystallization of Li_2SiO_3 and $Li_2Si_2O_5$ [13]. Hence, they [13] concluded that Li_3PO_4 does not nucleate lithium disilicate crystals, as previously studied for the glasses of similar composition [17].

However, in this case a different early phase formation was observed. Due to CaF_2 added in this system, the peaks were associated with the crystal of fluorapatite indexed in the XRD pattern in parallel with Li_3PO_4. Subsequently, at an early stage, the incorporation of fluorine in phosphate glasses leads to P-F bonds at the expense of P-O-P bonds to possibly form fluorapatite: $Ca_5(PO_4)_3F$ crystals [39]. Therefore, it is reasonable to conclude that the formation of $Li_2Si_2O_5$ crystals in this case occurred from the heterogeneous nucleation of Li_3PO_4 and $Ca_5(PO_4)_3F$ caused from the addition of CaF_2 and P_2O_5 in glass compositions. Hence, P_2O_5 also act as a nucleating agent in this system.

Furthermore, the investigation on spodumene, $Li_2O{\cdot}Al_2O_3{\cdot}4SiO_2$ glass ceramics adding ZrO_2 suggested that Al_2O_3 content should not exceed 30% wt to achieve

a low coefficient of thermal expansion and highly thermal shock resistant [40], as a result of detritions of mechanical strength [35]. In this study only 2% wt of Al_2O_3 was added in the glass compositions, in the range to produce a low thermal expansion coefficient glass ceramic.

3.4. Microstructure. The morphology of the system was studied, and SEM micrographs of the sample surfaces are shown in Figure 5. At 700°C, SEM images of glass ceramic LD1 illustrate the spherical-like crystals of both Li_2SiO_3 and Li_3PO_4. Normally, Li_2SiO_3 and Li_3PO_4 crystals could dissolve in HF solution if one-stage treatment applied due to the precipitate crystals was not stable [4]. In this study, two-stage treatment was applied, thus, Li_2SiO_3 and Li_3PO_4 crystals could be seen by SEM consistent with XRD pattern which indicated the formation of both crystals. XRD patterns also indicated the formation of the lithium aluminium silicate: virgilite and fluorapatite crystals. Both crystals have a rounded or spherical-like shape similar to Li_2SiO_3 and Li_3PO_4 but smaller in size, which is hardly to find by either SEM technique or energy dispersive spectroscopy (EDS) [41]. Transmission electron microscopy could be a better technique to show these spherical shapes of the virgilite and fluorapatite crystals [42, 43].

After heat treatment at 800°C, several lath-like crystals of lithium disilicate were observed. With increasing heat treatment temperature, the more and the coarser the lath-like crystals occurred, in close consistency with XRD results. A similar microstructure was also observed in LD2. A small discrepancy appeared at 750°C for LD2 in which no lath-like crystal of $Li_2Si_2O_5$ was noticed but the lath-like crystals can be observed in samples after heat treatment at 800°C and 850°C.

SEM images of LD3 and LD4 shown in Figures 5(c) and 5(d) reveal that the spherical-shaped crystals of both Li_2SiO_3 and Li_3PO_4 occurred at 700°C and 750°C followed by the appearance of needle-like crystals or plate-like crystals of $Li_2Si_2O_5$ in a glassy matrix at 800°C and 850°C. This needle-like crystal looked very long with a narrow diameter. The higher the temperature of heat treatment, the larger the aspect ratio and greater interlocking of the needle-like crystal was observed. The increase in the Si : Li ratio in LD3 and LD4 compositions seems to have induced the change in the microstructure of the $Li_2Si_2O_5$ crystal from the fine lath-like crystal to the needle-like or plate-like crystal. The addition of a slight amount of MgO content in glass composition showed no significant changes in the microstructure of the glass ceramics. This phenomenon was also observed in LD1 and LD2.

3.5. Mechanical Properties

3.5.1. Indentation Fracture Toughness (IFT). The IFT values of the glass ceramics LD1–LD4 at different temperatures are shown in Figure 6. The highest IFT for all samples was obtained at 800°C with glass ceramics LD1, LD2, and LD4, 3.59 ± 0.01, 3.72 ± 0.03, and 3.58 ± 0.01 MPa $m^{1/2}$, respectively, which suggests that this heat-treatment temperature is close to the optimum, probably caused by the finer and more highly interlocked crystals. Of exceptional note was that the highest IFT value of LD3, 7.88 ± 0.01 MPa $m^{1/2}$ was found in samples at a heat treatment of 850°C at which a finer microstructure with a high aspect ratio might be occurring. It was reported that the finer the microstructure, the more twisted the path for fracture and, therefore, the higher the fracture toughness [42]. Consequently, LD1, LD2, and LD4 at 850°C and LD3 at 800°C, which illustrated a coarser microstructure, obtained lower IFT values. As shown in (Figure 4(c)), XRD pattern of LD3 indicated the more numbers of lithium aluminium silicate: virgilite crystals with a high intensity compared to that of other glasses, particularly at 800°C and 850°C. Therefore, the thermal expansion mismatch between $Li_2Si_2O_5$ and virgilite resulted in residual stresses or microcracks on cooling, which create crack tip shielding and enhanced toughness of LD3 at 800C° and 850°C.

3.5.2. Biaxial Flexural Strength (BFS). Figure 7 presents the BFS values of the glass ceramics LD1-LD4 at different temperatures. For LD1, the BFS was at its maximum (396.24 ± 79 MPa) at 750°C which didnot significantly decrease after heat treatment at 800°C (388.05 ± 38 MPa) followed by drastical change to 256.06 ± 29 MPa at 850°C. In LD2, the maximum BFS was 471.39 ± 42 MPa at 800°C which increased from 383.62 ± 28 MPa at 750°C followed by a decrease to 295.55 ± 23 MPa at 850°C. In LD3, an increase in BFS was observed from 353.17 ± 81 MPa in samples heat-treated at 750°C to 404.94 ± 26 MPa at 800°C followed by a decrease to 317.01 ± 13 MPa at 850°C. For LD4, the maximum BFS was 489.73 ± 47 MPa at 800°C which sharply increased from 251.82 ± 20 MPa at 750°C followed by a decrease to 388.78 ± 39 MPa at 850°C. Overall, the highest BFS of the studied glass ceramics was found at 800°C in which a finer microstructure was noted. Another reason is that the thermal expansion mismatch between lithium disilicate and other phases, including glass matrix, probably caused tangential compressive stresses around the crystals, which was responsible for crack deflection and enhanced strength [1].

Irwin, as with Griffith approach, introduced stress intensity factors as a quantitative indicator on the effect of dimension and shape [44] on the magnitude of the stresses near a crack tip [45]. This is expressed in a general formula for an infinite plate with crack length = $2a$ at its center,

$$\sigma = \frac{K_{IC}}{\sqrt{\pi c}}, \tag{6}$$

where σ is the nominal stress or biaxial flexural strength, K_{IC} is the fracture toughness, and C is the flaw size.

With this formula, it is possible to find the correlation between strength and the stress field (fracture toughness) in the terms of a critical flaw size, as shown in Table 4 since both strength and fracture toughness are known. It is worth noting that Mencik [44] and Green [45] suggested that if the crack length or flaw size is smaller than the pore or crystal size, a high K_{IC} but low strength value may occur. This could explain the situation of the high fracture toughness but low in strength of LD3 at 800°C and 850°C due to the largest critical

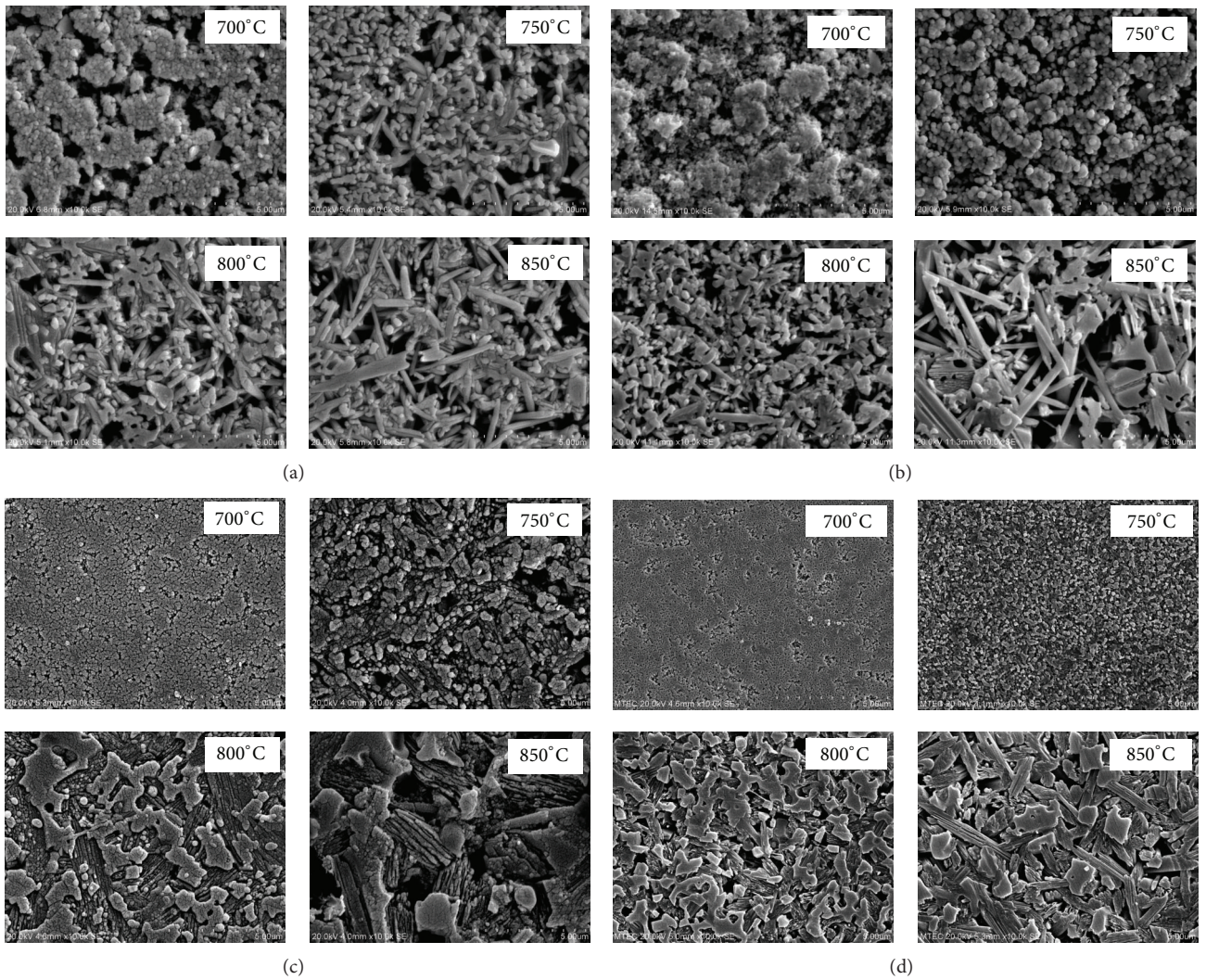

Figure 5: SEM micrographs of (a) LD1, (b) LD2, (c) LD3, and (d) LD4 after heat treatment at different temperatures for 2 hrs.

Table 4: The comparison on calculated flaw sizes of Glasses LD1–LD4 after being heat-treated at 750°C, 800°C, and 850°C.

Glasses	750°C			800°C			850°C		
	K_{IC} (MPa m$^{1/2}$)	σ (MPa)	C (μm)	K_{IC} (MPa m$^{1/2}$)	σ (MPa)	C (μm)	K_{IC} (MPa m$^{1/2}$)	σ (MPa)	C (μm)
LD1	1.80	396.24	6.56	3.59	388.05	27.25	2.69	256.06	35.21
LD2	1.91	383.62	7.86	3.72	471.39	19.81	2.30	295.55	19.31
LD3	1.44	353.17	5.26	7.25	404.94	102.17	7.88	317.01	196.87
LD4	1.19	251.82	7.10	3.58	489.73	16.98	2.76	388.78	16.03

flaw size (~102 μm for 800°C and ~197 μm for 850°C) which was found in these samples.

3.6. Chemical Solubility. Chemical solubility is an important property for dental restoration since a high solubility or low resistance to erosion will strictly limit the effective lifetime of the restoration. Moreover, the chemical solubility property also directly affects the strength of the glass ceramic material. Figure 8 shows the chemical solubility value of all glass ceramics at different temperatures. It was found that the chemical solubility of all glass ceramics slightly decreased with increasing temperature, except that of LD2 which had MgO content. The addition of alkaline earth such as CaO and MgO in glass composition could increase chemical solubility in glass ceramics owing to the increased volume of crystalline phase [6]. Considerably, the microstructure of LD2 at 850°C (Figure 5(d)) shows a high aspect ratio of needle-like crystals which are loosely interlocking compared to other glasses. This kind of microstructure might be easy for the acid to attack on the surface of the sample. Therefore, the microstructure could also be responsible for high chemical solubility of LD2.

In fact, the chemical solubility of the core ceramic materials must be less than 2000 μg/cm^2, and that of the body ceramic materials directly in contact with the oral

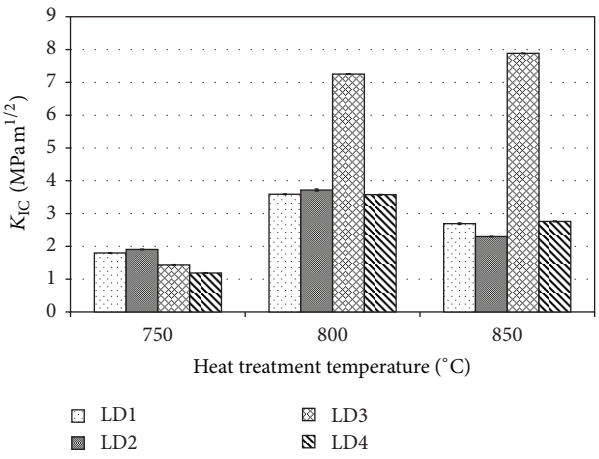

Figure 6: The fracture toughness of LD1, LD2, LD3, and LD4 heat treated at different temperatures for 2 hrs.

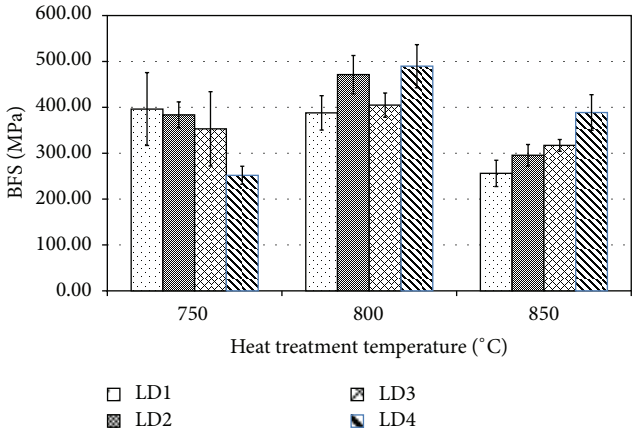

Figure 7: The biaxial flexural strength of LD1, LD2, LD3, and LD4 at different heat-treated temperatures for 2 hrs.

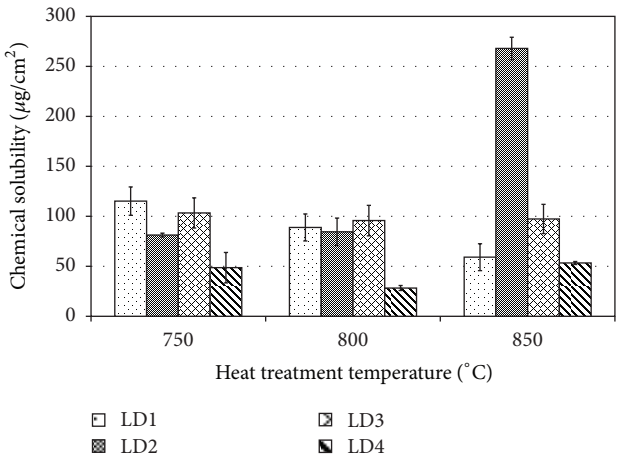

Figure 8: The chemical solubility of LD1, LD2, LD3, and LD4 at different heat-treated temperatures for 2 hrs.

environment should be less than 100 μg/cm^2 according to ISO 6872 [28]. Generally, the chemical solubility of the glass ceramic in this study was in the acceptable range according to ISO 6872 for core ceramic material. The lowest chemical durability was LD4, at ~28 μg/cm^2, heat-treated at 800°C.

4. Conclusions

All glass ceramics were identified by X–ray diffraction method, and it was found that P_2O_5 and CaF_2 served as a nucleating site for lithium phosphate, Li_3PO_4, and fluorapatite, $Ca_5(PO_4)_3F$, to induce heterogeneous nucleation and then produce a fine-grained interlocking microstructure of lithium disilicate glass ceramics. MgO content in this system seems to have played less of a role in changing the phase formation and microstructure of the glasses but enhanced the viscosity of the melting glass and thermal expansion coefficient including the chemical solubility. The increase in the Si : Li ratio in glass compositions resulted from the change in the microstructure of $Li_2Si_2O_5$ crystal from fine lath-like crystals to needle-like or plate-like crystals. In this study, LD3 heat-treated at 850°C exhibited the best fracture toughness of ~8 MPa m$^{1/2}$. In addition, LD4 heat-treated at 800°C had the best biaxial flexural strength and chemical solubility of ~490 MPa and ~28 μg/cm^2, respectively. These glass compositions are promising for potential use as dental crowns.

Conflict of Interests

There is no financial or other relationship that might be perceived as leading to a conflict of interests. The authors declare that there is no conflict of interests.

Acknowledgment

This work was performed with support from the National Metal and Materials Technology Center, Ministry of Science and Technology of Thailand, under Project no. 1100057.

References

[1] I. Denry and J. A. Holloway, "Ceramics for dental applications: a review," *Materials*, vol. 3, no. 1, pp. 351–368, 2010.

[2] E. El-Meliegy and R. van Noort, *Glasses and Glass Ceramics for Medical Applications*, Springer, New York, NY, USA, 2012.

[3] C. C. Gonzagaa, P. F. Cesara, C. Y. Okadaa, C. Fredericcib, F. B. Netob, and H. N. Yoshimurab, "Mechanical properties and porosity of dental glass-ceramics hot-pressed at different temperatures," *Materials Research*, vol. 11, no. 3, pp. 301–306, 2008.

[4] X. Zheng, G. Wen, L. Song, and X. X. Huang, "Effects of P_2O_5 and heat treatment on crystallization and microstructure in lithium disilicate glass ceramics," *Acta Materialia*, vol. 56, no. 3, pp. 549–558, 2008.

[5] G. H. Beall and R. C. Doman, *Glass-Ceramics in Corning Research*, Corning Glass Works Scientists, New York, NY, USA, 1987.

[6] P. W. McMillan, *Glass-Ceramics*, Academic Press, London, UK, 1979.

[7] P. Hing and P. W. McMillan, "A transmission electron microscope study of glass-ceramics," *Journal of Materials Science*, vol. 8, no. 3, pp. 340–348, 1973.

[8] P. F. James, "Kinetics of crystal nucleation in silicate glasses," *Journal of Non-Crystalline Solids*, vol. 73, no. 1-3, pp. 517–540, 1985.

[9] R. Ota, N. Mishima, T. Wakasugi, and J. Fukunaga, "Nucleation of Li_2O-SiO_2 glass and its interpretation based on a new liquid model," *Journal of Non-Crystalline Solids*, vol. 219, pp. 70–74, 1997.

[10] E. D. Zanotto, "Metastable phases in lithium disilicate glasses," *Journal of Non-Crystalline Solids*, vol. 219, pp. 42–48, 1997.

[11] L. L. Burgner, P. Lucas, M. C. Weinberg, P. C. Soares Jr., and E. D. Zanotto, "On the persistence of metastable crystal phases in lithium disilicate glass," *Journal of Non-Crystalline Solids*, vol. 274, no. 1, pp. 188–194, 2000.

[12] L. L. Burgner and M. C. Weinberg, "Assessment of crystal growth behavior in lithium disilicate glass," *Journal of Non-Crystalline Solids*, vol. 279, no. 1, pp. 28–43, 2001.

[13] W. Höland, V. Rheinberger, and M. Schweiger, "Control of nucleation in glass ceramics," *Philosophical Transactions of the Royal Society A*, vol. 361, no. 1804, pp. 575–589, 2003.

[14] J. M. Barrett, D. E. Clark, and L. L. Hench, "Glass-ceramic dental restoration," U.S. Patent 4,189,325, 1980.

[15] J. M. Wu, W. R. Cannon, and C. Panzera, "Castable glass-ceramic composition useful as dental restorative," U.S. Patent 4,515,634, 1985.

[16] D. U. Thlyaganov, S. Agathopoulos, I. Kansal, and P. Valerio, "Synthesis and properties of lithium disilicate glass-ceramics in the system SiO_2-Al_2O_3-K_2O-Li_2O," *Ceramics International*, vol. 35, no. 8, pp. 3013–3019, 2009.

[17] D. Holland, Y. Iqbal, P. James, and B. Lee, "Early stages of crystallisation of lithium disilicate glasses containing P_2O_5—an NMR study," *Journal of Non-Crystalline Solids*, vol. 232–234, pp. 140–146, 1998.

[18] L. M. Echeverria and G. H. Beall, "New lithium disilicate glass-ceramics," *Boletin de la Sociedad Espanola de Ceramica y Vidrio*, vol. 5, pp. 183–188, 1999.

[19] G. H. Beall, "Glass-ceramics: recent development and application," *Ceramic Transactions*, vol. 30, pp. 241–266, 1993.

[20] G. N. Beall, "Design of glass-ceramics," *Solid State Sciences*, vol. 3, pp. 333–354, 1989.

[21] S. C. von Clausbruch, M. Schweiger, W. Höland, and V. Rheinberger, "The effect of P_2O_5 on the crystallization and microstructure of glass-ceramics in the SiC_2-Li_2O-K_2O-ZnO-P_2O_5 system," *Journal of Non-Crystalline Solids*, vol. 263-264, pp. 388–394, 2000.

[22] Y. Iqbal, W. E. Lee, D. Holland, and P. F. James, "Crystal nucleation in P_2O_5-doped lithium disilicate glasses," *Journal of Materials Science*, vol. 34, no. 18, pp. 4399–4411, 1999.

[23] T. Kasuga, T. Kimata, and A. Obata, "Preparation of a calcium titanium phosphate glass-ceramic with improved chemical durability," *Journal of the American Ceramic Society*, vol. 92, no. 8, pp. 1709–1712, 2009.

[24] G. H. Beall, "Glass-ceramics: recent development and application," in *Nucleation and Crystallization in Glasses and Liquids. Ceramic Transactions*, M. C. Weinberg, Ed., vol. 30, pp. 241–266, American Ceramics Society, Westerville, Ohio, USA, 1993.

[25] M. Schweiger, M. Frank, S. Cramer von Clausbruch, W. Holand, and V. Rheinberger, "Microstructure and properties of presses glass-ceramic core to zirconia post," *Quintessence of Dental Technology*, vol. 22, pp. 143–152, 1998.

[26] M. Frank, M. Schweiger, V. Rheinberger, and W. Holand, "High strength translucent sintered glass-ceramic for dental application," *Glasstech. Ber. Glass Science Technology*, vol. 71C, pp. 345–348, 1998.

[27] R. Morrell, *Biaxial Flexural Strength Testing of Ceramic Materials*, National Physical Laboratory, Teddington, Middlesex, UK, 1998.

[28] "Dentistry—Ceramic materials," Part 4, types, classes and their identification, ISO 6872:2008.

[29] M. Schweiger, W. Holand, M. Frank, H. Drescher, and V. Rheinberger, "IPS Empress®2: a new pressable high strength glass-ceramic for esthetic all ceramic restoration," *Quintessence of Dental Technology*, vol. 22, pp. 143–152, 1999.

[30] S. M. Salman and S. N. Salama, "Crystallization and thermal expansion characteristics of In_2O_3-containing lithium iron silicate-diopside glasses," *Ceramics—Silikaty*, vol. 55, no. 2, pp. 114–122, 2011.

[31] H. Darwish, S. N. Salama, and S. M. Salman, "Contribution of germanium dioxide to the thermal expansion characteristics of some borosilicate glasses and their corresponding glass-ceramics," *Thermochimica Acta*, vol. 374, no. 2, pp. 129–135, 2001.

[32] R. H. Hopkins, D. H. Damon, P. Piotrowski, M. S. Walker, and J. H. Uphoff, "Thermal properties of synthetic fluorapatite crystals," *Journal of Applied Physics*, vol. 42, no. 1, pp. 272–275, 1971.

[33] P. McAlinn, D. E. Clark, and L. L. Hench, "High expansion glass-cermaic articles," U.S. Patent 4,480,044, 1984.

[34] B. M. French, P. A. Jezek, and D. E. Appleman, "Virgilite: a new lithium aluminum silicate mineral from the Macusani glass, Peru," *American Mineralogist*, vol. 63, pp. 461–465, 1978.

[35] Z. Strnad, *Glass-Ceramic Materials in Glass Science and Technology*, Elsevier, Amsterdam, The Netherlands, 1986.

[36] W. Höland and G. H. Beall, *Glass-Ceramic Technology*, The American Ceramic Society, Westerville, Ohio, USA, 2002.

[37] P. Goharian, A. Nemati, M. Shabanian, and A. Afshar, "Properties, crystallization mechanism and microstructure of lithium disilicate glass-ceramic," *Journal of Non-Crystalline Solids*, vol. 356, no. 4-5, pp. 208–214, 2010.

[38] G. Wen, X. Zheng, and L. Song, "Effects of P_2O_5 and sintering temperature on microstructure and mechanical properties of lithium disilicate glass-ceramics," *Acta Materialia*, vol. 55, no. 10, pp. 3583–3591, 2007.

[39] A. W. A. El-Shennawi, A. A. Omar, and E. M. A. Hamzawy, "Role of fluorine and phosphorus in the crystallisation of K-fluorricherite glass," in *Proceedings of the 18th International Congress on Glass*, American Ceramic Society, San Francisco, Calif, USA, 1998.

[40] A.-X. Lu, M. Jia, and S.-J. Liu, "Effects of heat treatment temperature on crystallization and thermal expansion coefficient of Li_2O-Al_2O_3-SiO_2," *Journal of Central South University of Technology*, vol. 11, no. 3, pp. 235–238, 2004.

[41] Z. Xiao, J. Zhou, Y. Wang, and M. Luo, "Microstructure and properties of Li_2O-Al_2O_3-SiO_2-P_2O_5 glass-ceramics," *Open Materials Science Journal*, vol. 5, pp. 45–50, 2011.

[42] M. Mirsaneh, I. M. Reaney, P. V. Hatton, and P. F. James, "Characterization of high-fracture toughness K-fluorrichterite-fluorapatite glass ceramics," *Journal of the American Ceramic Society*, vol. 87, no. 2, pp. 240–246, 2004.

[43] N. Kanchanarat, S. Bandyopadhyay-Ghosh, I. M. Reaney, I. M. Brook, and P. V. Hatton, "Microstructure and mechanical

properties of fluorcanasite glass-ceramics for biomedical applications," *Journal of Materials Science*, vol. 43, no. 2, pp. 759–765, 2008.

[44] J. Mencik, *Strength and Fracture of Glass and Ceramics*, Elsevier, Amsterdam, The Netherlands, 1992.

[45] D. J. Green, *An Introduction to the Mechanical Properties of Ceramics*, Cambridge University Press, Cambridge, UK, 1998.